Dynamic correspondence principle in the viscoelasticity of metallic glasses

Guo-Jian Lyu, Ji-Chao Qiao, Yao Yao, Jean-Marc Pelletier, David Rodney, Julien Morthomas, Claudio Fusco

Dear author,

Please note that changes made in the online proofing system will be added to the article before publication but are not reflected in this PDF.

We also ask that this file not be used for submitting corrections.

Scripta Materialia xxx (xxxx) xxx

Contents lists available at ScienceDirect

Scripta Materialia

journal homepage: www.elsevier.com/locate/scriptamat

Dynamic correspondence principle in the viscoelasticity of metallic glasses

Guo-Jian Lyu [a,b], Ji-Chao Qiao [a,b], Yao Yao [a,c,*], Jean-Marc Pelletier [b], David Rodney [d], Julien Morthomas [b], Claudio Fusco [b,**]

[a] School of Mechanics, Civil Engineering Architecture, Northwestern Polytechnical University, Xi'an 710072, PR China
[b] Université de Lyon, MATEIS, UMR CNRS 5510, INSA-Lyon, F-69621 Villeurbanne cedex, France
[c] Max Planck Inst Eisenforsch GmbH, Max Planck Str 1, D-40237 Dusseldorf, Germany
[d] Institut Lumière Matière, UMR5306 Université Lyon 1-CNRS, Université de Lyon, F-69622 Villeurbanne Cedex, France

ARTICLE INFO

Article history:
Received 2 July 2019
Accepted 11 August 2019
Available online xxxx

Keywords:
Metallic glass
Dynamic mechanical relaxations
Molecular dynamics simulations
Dynamic correspondence principle
Viscoelasticity
Dynamic Poisson's ratio

ABSTRACT

We simulate dynamical mechanical spectroscopy in a $Cu_{64}Zr_{36}$ bulk metallic glass using non-equilibrium molecular dynamics. Applying several loading conditions (constant volume, longitudinal, uniaxial and isostatic), we find that different elastic moduli have very contrasted dynamical properties but satisfy the dynamic correspondence principle, which states that the relations between static moduli can be extended to dynamical moduli, both below and above the glass transition temperature. In particular, we determine the debated dynamic Poisson's ratio from three different but consistent expressions. Finally, we trace the origin of dissipation down to regions of low stability devoid of icosahedral clusters.

Dynamic mechanical spectroscopy (DMS) is a widespread method to measure complex dynamic elastic moduli and characterize the viscoelastic properties of materials [1]. In the case of metallic glasses (MGs) of particular interest here [2], DMS has been used to evaluate internal friction, i.e. the energy dissipated during cyclic deformation, a key engineering parameter for a number of applications such as resonating micro-electromechanical systems (MEMS) [3]. On a more fundamental level, DMS has also been used to study the intricate relaxation dynamics characteristic of disordered solids [4,5] and in particular the primary (α) and secondary (β) relaxations [4,6].

Experimentally, two modes of deformation are applied, bending [7–9] and torsion [10–12], giving access respectively to the complex Young and shear moduli. DMS has also been simulated using non-equilibrium molecular dynamics (NEMD) [13–17]. The simulations are limited to rather high frequencies (>1 GHz) but allow to simultaneously measure the dissipation and analyze its origin at the atomic level. In particular, it has been shown that in metallic glasses, atoms with stable icosahedral environments do not participate in dissipation [13].

In the static limit, there are only two independent elastic moduli in isotropic media [18]. They come as pairs, such as (λ, G), with λ Lamé's first parameter and G the shear modulus, and (E, ν), with E Young's modulus and ν Poisson's ratio. These moduli are related to one another, with for instance, $G = E/2(1+\nu)$. Therefore, if one can measure any two moduli, all other moduli are known. These relations are well established in static elasticity and derive from Hooke's law. It has been assumed that they also hold true in the dynamic case, through the so-called dynamic correspondence principle [19,20], which simply means that real static moduli can be replaced by their complex dynamic counterparts. However, concerns have been raised about the dynamic Poisson's ratio [21–24]. Also, the correspondence principle has actually never been tested experimentally because it requires a precision on the complex moduli very difficult to reach [21]. It has also not been tested in NEMD, which to the best of our knowledge, has so far only been applied with shear deformations. At high frequencies, in the harmonic regime, the dynamic elastic moduli can be expressed analytically [25] and satisfy the correspondence principle. However, the same is far from clear in the anharmonic regime observed in MGs.

Here, we consider a typical CuZr MG and use NEMD to apply different loading geometries and test the dynamic correspondence principle over a wide range of frequencies and temperatures. We find that different elastic moduli exhibit very different dynamic properties but that the correspondence principle applies both below and above the glass transition temperature. We also devote a special discussion to the complicated case of Poisson's ratio.

The MD simulations were performed using the open source LAMMPS package [26]. We considered a $Cu_{64}Zr_{36}$ MG, which has a high glass forming ability and has been widely investigated by MD simulations in the past [27–32]. The interatomic interactions are based on the EAM potential developed by Mendelev et al. [33]. We simulated a

* Correspondence to: Y. Yao, School of Mechanics, Civil Engineering Architecture, Northwestern Polytechnical University, Xi'an 710072, PR China.
** Corresponding author.
E-mail addresses: yaoy@nwpu.edu.cn (Y. Yao), claudio.fusco@insa-lyon.fr (C. Fusco).

https://doi.org/10.1016/j.scriptamat.2019.08.015
1359-6462/

glass with 108,000 atoms (see Fig. 1(a)), obtained by quenching a liquid from 2000 K down to 100 K with a typical quenching rate of 10^{11} K/s, keeping the pressure to zero during the cooling procedure.

We simulated DMS using the same methodology as in previous NEMD works [13,16,25]. Fig. 1 illustrates the case of pure shear. The sample was first equilibrated at the target temperature and zero pressure for 1 ns. As shown in Fig. 1(a), we then applied a sinusoidal strain $\varepsilon_{xx}(t) = \varepsilon_A \sin(\omega t)$ along the X direction, with ε_A and $T_\omega = 2\pi/\omega$, the amplitude and period of the cyclic deformation. In order to impose a pure shear and keep the volume of the cell constant, we applied strains $\varepsilon_{yy}(t) = \varepsilon_{zz}(t) = -0.5\varepsilon_{xx}(t)$ along the Y and Z directions. We tested different strain amplitudes (see Supplementary materials) and found $\varepsilon_A = 2.5\%$ an optimal value, small enough to remain in the elastic regime but large enough to avoid a poor signal-to-noise ratio at high temperatures. We also simulated different numbers of cycles (see Supplementary materials), and found that 5 cycles are enough to measure accurately dynamic elastic moduli. The variation of the stress tensor was recorded during the deformation. As illustrated in Fig. 1(a), after shifting all values by periodicity in the first period, we fitted the stress in the X direction as $\sigma_{xx}(t) = \sigma_0 + \sigma_A \sin(\omega t + \delta)$, with σ_A the stress amplitude and δ the phase shift. Discarding the small offset stress σ_0, we have in complex notation, $\sigma_{xx}(t) = \sigma_A/\varepsilon_A \exp(i\delta)\varepsilon_{xx}(t)$. According to Hooke's law:

$$\boldsymbol{\sigma} = 2G\boldsymbol{\varepsilon} + \lambda Tr(\boldsymbol{\varepsilon})I \quad (1)$$

which in the present case of pure shear where $\mathrm{Tr}(\boldsymbol{\varepsilon}) = 0$ yields $\sigma_{xx} = 2G\varepsilon_{xx}$. The dynamic shear modulus is thus $G^* = 0.5\sigma_A/\varepsilon_A \exp(i\delta)$, with the storage and loss moduli given by the real and imaginary parts of G^*: $G' = 0.5\sigma_A/\varepsilon_A \cos(\delta)$ and $G'' = 0.5\sigma_A/\varepsilon_A \sin(\delta)$. We note also that according to Hooke's law (Eq. (1)), we should have $\sigma_{yy}(t) = \sigma_{zz}(t) = -0.5\sigma_{xx}(t)$, which is readily tested in Fig. 1(b).

Fig. 1(c) shows the storage G' and loss G'' shear moduli as a function of temperature. Similar results were obtained by Yu et al. [13]. The storage and loss moduli are highly dependent on the loading frequencies, with an α-relaxation peak in G'' close to the glass transition temperature, which shifts to higher temperature as the frequency increases, in agreement with experiments [4,6,34].

At variance with previous works, which considered only shear deformations, we applied four different loading conditions, shown schematically in Fig. 2(a):

(1) Constant volume: application of sinusoidal strains $\varepsilon_{xx}(t) = -2\varepsilon_{yy}(t) = -2\varepsilon_{zz}(t)$ to obtain the shear modulus G^*, as discussed above.
(2) Uniaxial deformation: application of a sinusoidal strain along the X direction and maintain $\sigma_{yy}(t) = \sigma_{zz}(t) = 0$ to obtain Young's modulus, E^*, defined as $\sigma_{xx}(t) = E^*\varepsilon_{xx}(t)$.
(3) Longitudinal deformation: application of a sinusoidal strain along the X direction and maintain the Y and Z dimensions unchanged to obtain the longitudinal modulus, M^*, defined as $\sigma_{xx}(t) = M^*\varepsilon_{xx}(t)$.
(4) Isostatic deformation: application of the same sinusoidal strain along the X, Y and Z directions simultaneously to obtain the bulk modulus K^* defined as $P(t) = -(\sigma_{xx}(t) + \sigma_{yy}(t) + \sigma_{zz}(t))/3 = -3K^*\varepsilon(t)$.

Fig. 2(b) and (c) show the amplitude of the complex moduli σ_A/ε_A and the phase shifts obtained with the different loading conditions. They have opposite hierarchies: a loading condition, which strongly constrains the deformation, such as an isostatic deformation, yields a high σ_A/ε_A ratio, and a small phase shift and vice versa for a weakly constraining loading, such as uniaxial loading. We also find as expected that above the α-relaxation peak, when the system is no longer a glass but is in the supercooled region, Young's and shear moduli drop down to zero and their phase shift increases to almost π/2, i.e. the system is now a viscous liquid. But way of contrast, the bulk and longitudinal moduli remain finite at all temperatures, with negligibly small phase shifts.

Hooke's law (Eq. (1)) imposes relations between the elastic moduli as listed in Table. 1. For instance, for the longitudinal deformation, $\boldsymbol{\varepsilon} = \begin{pmatrix} \varepsilon & 0 & 0 \\ 0 & 0 & 0 \\ 0 & 0 & 0 \end{pmatrix}$, such that, from Hooke's law, $\sigma_{xx} = (2G + \lambda)\varepsilon$, $\sigma_{yy} = \sigma_{zz} = \lambda\varepsilon$. We therefore have $M = 2G + \lambda$ and λ is obtained by monitoring σ_{yy} and σ_{zz}. Fig. 3(a) and (b) show the evolution of M^* and λ^* from the NEMD simulations. If the dynamic correspondence

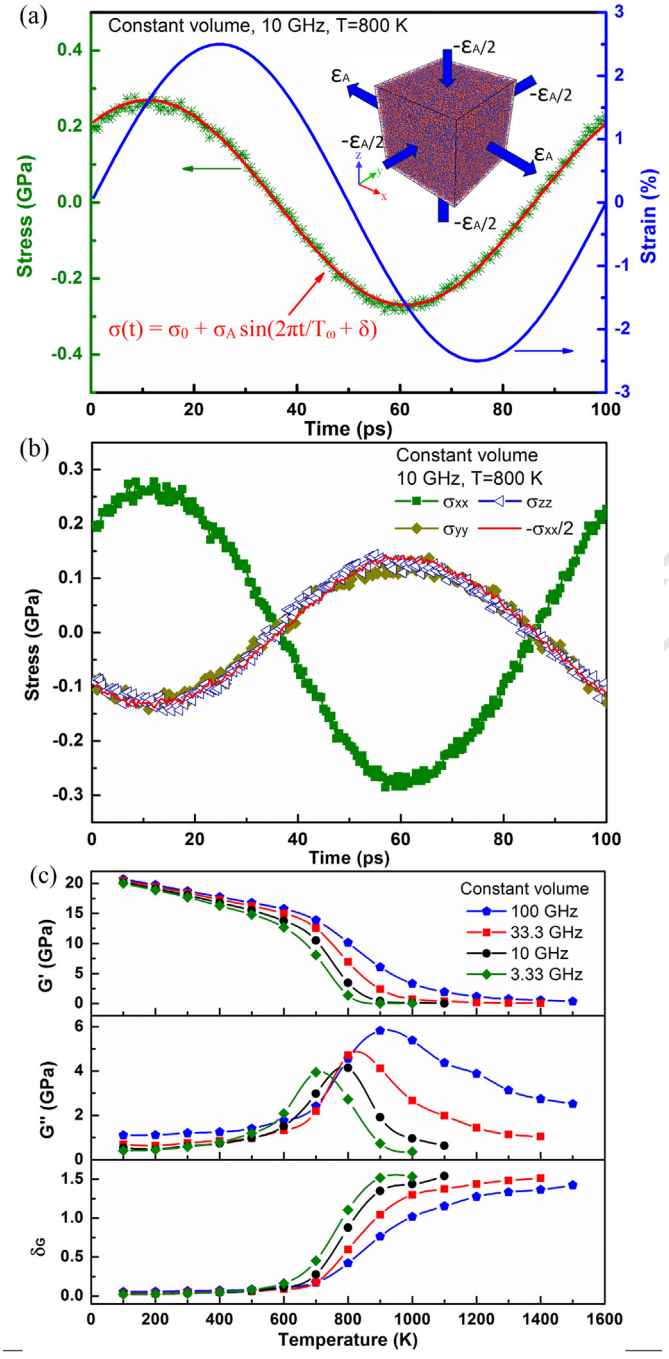

Fig. 1. Viscoelasticity in pure shear: (a) Time-dependent applied strain and resulting stress in X direction at 800 K and a frequency of 10 GHz ($T_\omega = 100$ ps). The inset shows the atomic configuration and a schematic of the loading. (b) Tensile stresses in all three directions. (c) Storage shear modulus G', loss modulus G'' and phase shift δ_G as a function of temperature for different loading frequencies noted in the figure.

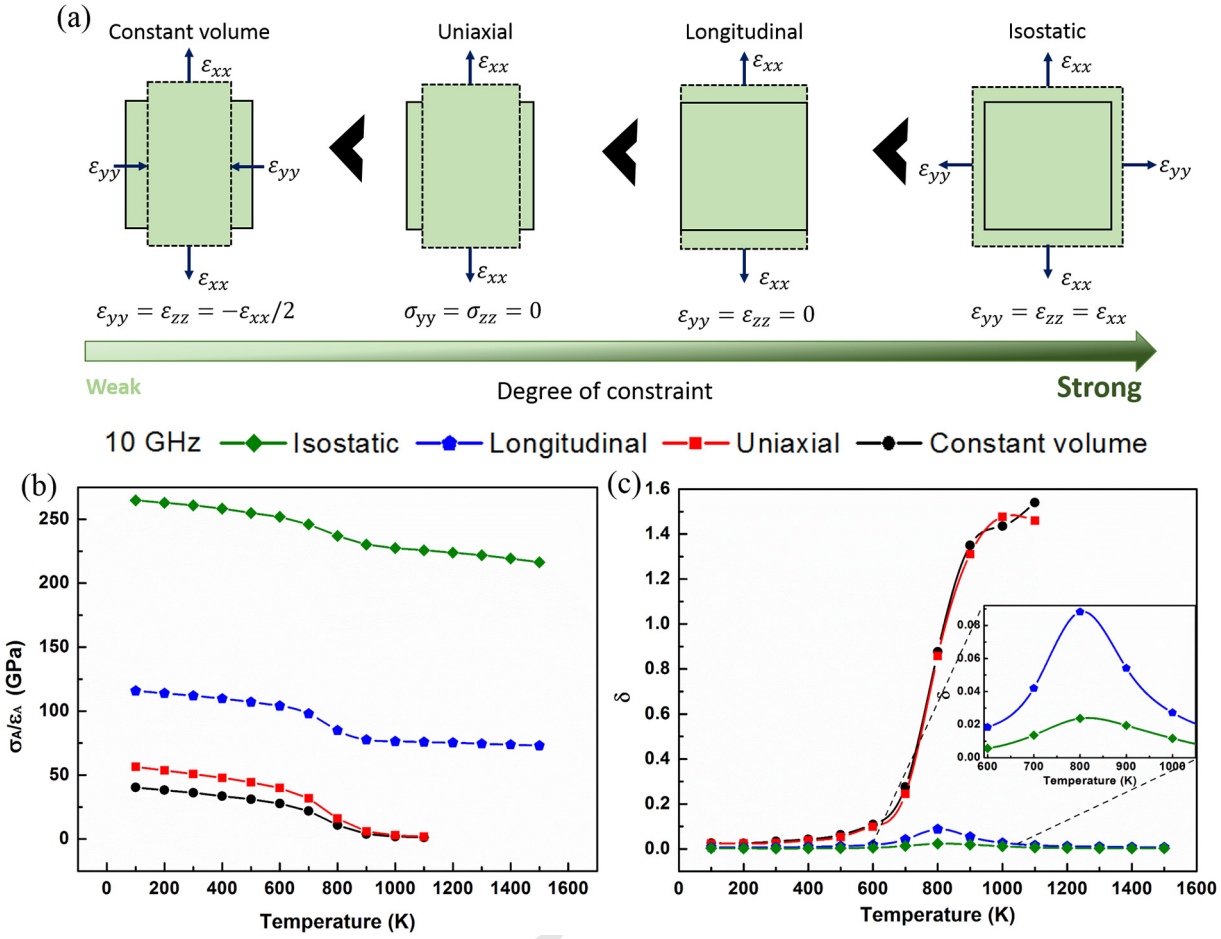

Fig. 2. (a) Schematic representation of the four loading conditions applied in NEMD simulations. (b) and (c) Amplitude of the complex moduli σ_A/ε_A and phase shifts for the four loading conditions at a frequency of 10 GHz.

principle holds, we should have $M^* = 2G^* + \lambda^*$, or equivalently, $G^* = (M^* - \lambda^*)/2$, which can be compared to the direct measurement of G^* by constant volume deformation. The comparison is done in Fig. 3(c), which shows that the above relation indeed holds at all temperatures. We note that λ^* is mostly independent of both the temperature and the frequency, with negligible λ'' and phase shift. As a result, there is a constant offset between M' and $2G'$ and $M'' \cong 2G''$. Similarly, in Fig. 3(d), we verify that $K^* = \lambda^* + 2G^*/3$. It may not be surprising that these relations satisfy the correspondence principle since they are linear. More complicated is the case of Young's modulus, which is expressed as $E^* = G^*(3\lambda^* + 2G^*)/(\lambda^* + G^*)$. However, Fig. 3(e) shows that this dynamic relation is also verified.

We now turn our attention to the dynamic Poisson's ratio, which has been debated in the literature because it may be defined in different ways [24]. We note that the ratio $\varepsilon_{yy}(t)/\varepsilon_{xx}(t)$ is not sinusoidal and therefore cannot be used to define Poisson's ratio. Instead, we use the ratio of complex strains, $\nu^* = -\varepsilon_{yy}^*/\varepsilon_{xx}^*$. This definition is compared in Fig. 3(f) with two expressions obtained from the correspondence principle: $\nu^* = \lambda^*/2(\lambda^* + G^*)$ and $\nu^* = 0.5 - E^*/6K^*$. All three expressions lead to the same result, further confirming the reliability of the correspondence principle. We see that ν' reaches 0.5 in the supercooled regime, i.e. the liquid is incompressible. Also, ν'' and δ_ν are negative, which implies that the transverse strain lags behind the longitudinal strain under dynamic loading, as expected due to damping effects [35]. A negative δ_ν is also consistent with λ'' being negligibly small as seen above, since in this case, $\tan\delta_\nu \simeq -G''/(\lambda' + G')$. Negative δ_ν were observed in previous experimental works, directly measuring the dynamic Poisson's ratio of several polymers [23,35]. Since the phase shift is very small, an extreme accuracy of the measurements is needed and some works have also reported zero phase shift [36,37].

Atomic mobility is the key to understand structural relaxation in MGs [13]. Fig. 4(a) shows an example of non-affine atomic displacements between the end of the 1st and the 5th cycles, when the cell is back to its original shape and there is no displacement induced by the applied homogeneous deformation. Atoms in different regions have very different mobilities, as expected from dynamic heterogeneities [38]. Following the work of Yu et al. [13], we define "faster atoms" as having displacements larger than 1.4 Å, half the average nearest neighbor distance. The "slow atoms" shown in Fig. 4(b) have almost reversible displacements under the deformation, and therefore contribute only to the elastic deformation of the MG. Conversely, the "faster atoms" undergo irreversible movements during the loading, i.e. inelastic deformation, which leads to energy dissipation. To further reveal the structural origin of the dynamic heterogeneity, Fig. 4(c) shows the Cu atoms with Voronoi index ⟨0,0,12,0⟩, identified as the central atoms of full icosahedral clusters. By deleting the isolated atoms with a cutoff 3.7 Å (the first minimum of the radial distribution

Table 1
Conversion formulas of elastic constants for homogenous isotropic materials.

	K	E	M	ν
(λ, G)	$\lambda + \frac{2G}{3}$	$\frac{G(3\lambda+2G)}{\lambda+G}$	$\lambda + 2G$	$\frac{\lambda}{2(\lambda+G)}$
(K, E)	K	E	$\frac{3K(3K+E)}{9K-E}$	$\frac{3K-E}{6K}$

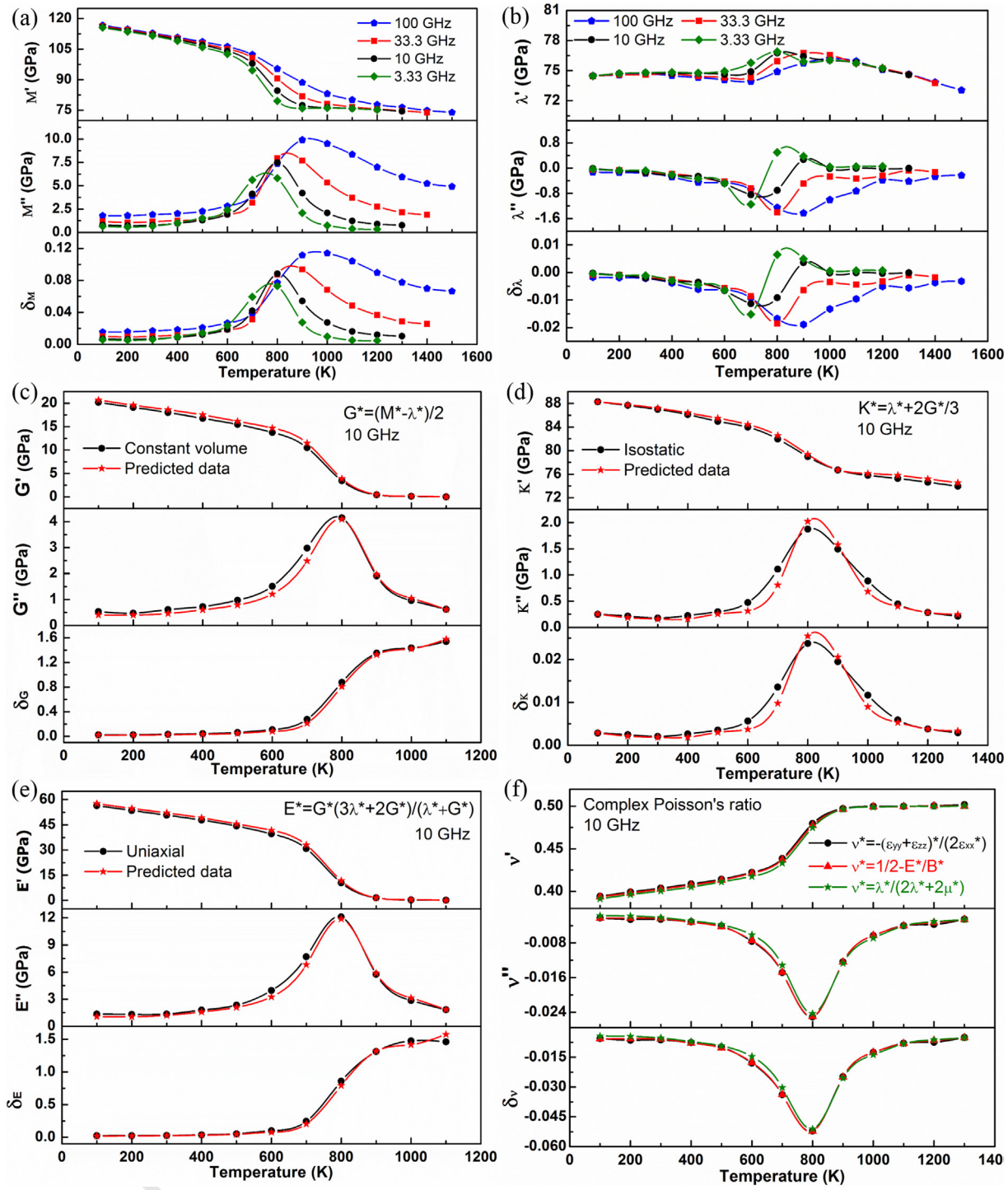

Fig. 3. Temperature dependence of measured and predicted complex moduli: (a) Longitudinal modulus M^* and (b) Lamé's first parameter λ^* obtained with NEMD at various frequencies, (c)–(f) Predictions of the complex shear, bulk, Young's moduli and Poisson's ratio using the dynamic correspondence principle (red data), compared with direct NEMD data (black data) at 10 GHz. (For interpretation of the references to color in this figure legend, the reader is referred to the web version of this article.)

function), not only the "slow atoms" on the surface of the simulation box but also the atoms with reversible movements inside the box match very well, as shown comparing Fig. 4(b) and (d). This result is consistent with the work of Yu et al. [13]. It can be concluded that the Cu-centered full icosahedral clusters in CuZr MG are stable and have a low atomic mobility, contributing to the stored elastic energy in each loading cycle. Conversely, most other atoms have larger mobilities and undergo irreversible inelastic displacements, contributing to the viscoelastic component and the energy dissipated in each loading cycle.

In summary, our results provide a numerical verification of the dynamic correspondence principle by investigating $Cu_{64}Zr_{36}$ MG in NEMD simulations. The resulting relationships between the viscoelastic complex moduli provide a guidance for engineering applications of viscoelastic materials under multi-axial stress conditions. Moreover, a well-posed definition of dynamic Poisson's ratio is highlighted. Spatially, the Cu-centered icosahedral clusters are found stable under cyclic deformation, contributing to the elastic component of the deformation, while most other atoms undergo irreversible displacements and

Please cite this article as: G.-J. Lyu, J.-C. Qiao, Y. Yao, et al., Dynamic correspondence principle in the viscoelasticity of metallic glasses, Scripta Materialia, https://doi.org/10.1016/j.scriptamat.2019.08.015

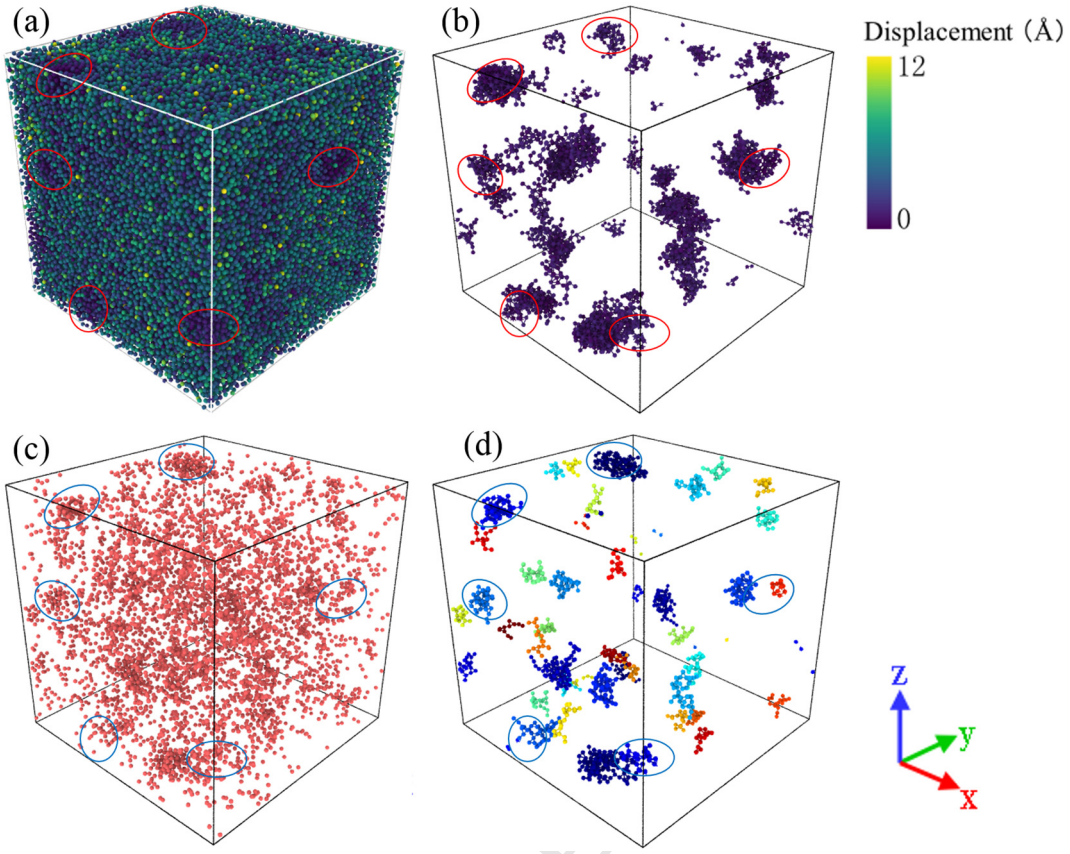

Fig. 4. (a) Atomic displacements between the end of the 1st and the 5th cycles at 800 K and 10 GHz under uniaxial deformation. (b) Same as (a) when atoms with displacements <1.4 Å and isolated atoms are removed. (c) Spatial distribution of Cu atoms with icosahedral environments. (d) Same as (c) when isolated icosahedral Cu atoms are removed. The Cu atoms are grouped in clusters shown with different colors for better display. The encircled regions indicate "slow atoms" that can be directly observed on the surface of the simulation box in (a).

contribute to the viscoelastic part. Our findings make a contribution to better understand the dynamic mechanical relaxations of MGs and also convey important information on the microstructural processes occurring during the glass transition.

Acknowledgements

This work was performed using HPC resources from the FLMSN, "Fédération Lyonnaise de Modélisation et Sciences Numériques", partner of EQUIPEX EQUIP@MESO. GJL acknowledges China Scholarship Council (CSC) for the scholarship. The research of JCQ was supported by the Fundamental Research Funds for the Central Universities (Nos. 3102018ZY010 and 3102017JC01003). YY acknowledges the Alexander von Humboldt Foundation for supporting his stay at Max-Planck-Institut für Eisenforschung.

Appendix A. Supplementary data

Supplementary data to this article can be found online at https://doi.org/10.1016/j.scriptamat.2019.08.015.

References

[1] K.P. Menard, Dynamic Mechanical Analysis: A Practical Introduction, CRC press, Boca Raton, Florida, 2008.
[2] M.W. Chen, NPG Asia Mater. 3 (2011) 82–90.
[3] X.Q. Zhou, D.Y. Yu, X.Y. Shao, S.Q. Zhang, S. Wang, Compos. Struct. 136 (2016) 460–480.
[4] J.C. Qiao, J.M. Pelletier, J. Mater. Sci. Technol. 30 (2014) 523–545.
[5] J.C. Qiao, Q. Wang, J.M. Pelletier, H. Kato, R. Casalini, D. Crespo, E. Pineda, Y. Yao, Y. Yang, Prog. Mater. Sci. 104 (2019) 250–329.
[6] H.B. Yu, W.H. Wang, K. Samwer, Mater. Today 16 (2013) 183–191.
[7] G.J. Lyu, J.C. Qiao, J. Gu, M. Song, J.-M. Pelletier, Y. Yao, J. Alloy. Compd. 769 (2018) 443–452.
[8] M. Lee, Y. Li, Y. Feng, C. Carter, Intermetallics 10 (2002) 1061–1064.
[9] X. Liu, B. Zhang, P. Wen, W. Wang, J. Non-Cryst. Solids 352 (2006) 4013–4016.
[10] G.J. Lyu, J.C. Qiao, J.M. Pelletier, Y. Yao, Mater. Sci. Eng. A 711 (2018) 356–363.
[11] J.C. Qiao, J.M. Pelletier, J. Appl. Phys. 112 (2012), 033518.
[12] J.C. Qiao, Y. Yao, J.M. Pelletier, L.M. Keer, Int. J. Plast. 82 (2016) 62–75.
[13] H.-B. Yu, K. Samwer, Phys. Rev. B 90 (2014), 144201.
[14] B.S. Shang, J. Rottler, P.F. Guan, J.-L. Barrat, Phys. Rev. Lett. 122 (2019), 105501.
[15] N.V. Priezjev, Comput. Mater. Sci. 153 (2018) 235–240.
[16] R. Ranganathan, Y. Shi, P. Keblinski, Phys. Rev. B 95 (2017), 214112.
[17] Z.D. Sha, L.C. He, Q.X. Pei, Z.S. Liu, Y.W. Zhang, T.J. Wang, Scr. Mater. 83 (2014) 37–40.
[18] L.D. Landau, E. Lifshiëtis, A. Kosevich, L. Pitaevskiæi, Theory of Elasticity, Pergamon Press, Oxford, 1986.
[19] W.T. Read, J. Appl. Phys. 21 (1950) 671–674.
[20] N.W. Tschoegl, The Phenomenological Theory of Linear Viscoelastic Behavior: An Introduction, Springer Science & Business Media, Berlin Heidelberg, 2012.
[21] N.W. Tschoegl, W.G. Knauss, I. Emri, Mech. Time-Depend. Mat. 6 (2002) 3–51.
[22] R.S. Lakes, A. Wineman, J. Elast. 85 (2006) 45–63.
[23] M. Giovagnoni, Mech. Mater. 17 (1994) 33–46.
[24] H.H. Hilton, Mater. Sci. Appl. 8 (2017) 291.
[25] T. Damart, A. Tanguy, D. Rodney, Phys. Rev. B 95 (2017), 054203.
[26] S. Plimpton, J. Comput. Phys. 117 (1995) 1–19.
[27] D. Wang, Y. Li, B.B. Sun, M.L. Sui, K. Lu, E. Ma, Appl. Phys. Lett. 84 (2004) 4029–4031.
[28] D. Xu, B. Lohwongwatana, G. Duan, W.L. Johnson, C. Garland, Acta Mater. 52 (2004) 2621–2624.
[29] S.D. Feng, L. Qi, L.M. Wang, S.P. Pan, M.Z. Ma, X.Y. Zhang, G. Li, R.P. Liu, Acta Mater. 95 (2015) 236–243.
[30] S.D. Feng, L. Qi, L.M. Wang, P.F. Yu, S.L. Zhang, M.Z. Ma, X.Y. Zhang, Q. Jing, K.L. Ngai, A.L. Greer, G. Li, R.P. Liu, Scr. Mater. 115 (2016) 57–61.
[31] T. Brink, M. Peterlechner, H. Roesner, K. Albe, G. Wilde, Phys. Rev. Appl. 5 (2016), 054005.
[32] Y.Q. Cheng, E. Ma, Prog. Mater. Sci. 56 (2011) 379–473.
[33] V. Borovikov, M.I. Mendelev, A.H. King, Model. Simul. Mater. Sci. Eng. 24 (2016), 085017.
[34] J.C. Qiao, J. Cong, Q. Wang, J.M. Pelletier, Y. Yao, J. Alloy. Compd. 749 (2018) 262–267.
[35] T. Pritz, Appl. Acoust. 60 (2000) 279–292.
[36] P.S. Dubbelday, J. Acoust. Soc. Am. 91 (1992) 1737–1744.
[37] G. Ledon, J. Derouet, J. Sound Vib. 89 (1983) 155–167.
[38] L. Berthier, Physics 4 (2011) 42.